Experimental and numerical investigation of direct two phase cooling for semiconductors

Antoine Loehrmann, Étienne Videcoq, Vincent Ayel, Sébastien Dutour, Stéphane Blanco, Benjamin Piaud, Vincent Forest, Olivier Crépel

International Conference on More Electric Aircraft
Towards greener aviation
Toulouse, February 7-8, 2024

Experimental and numerical investigation of direct two phase cooling for semiconductors

Antoine Loehrmann (1), Etienne Videcoq (2), Vincent Ayel (2),
Sébastien Dutour (3), Stéphane Blanco (3), Benjamin Piaud (4), Vincent Forest (4), Olivier Crepel (1)
1 : Airbus SAS – 1XRE, 2 rond-point Emile Dewoitine, 31700 Blagnac, France antoine.loehrmann@airbus.com
2 : Institut PPRIME, CNRS-ENSMA-Université de Poitiers, 86360 Futuroscope-Chasseneuil, France
etienne.videcoq@ensma.fr
3 : LAPLACE, UPS, INPT, CNRS, Université de Toulouse, 31555 Toulouse, France
sebastien.dutour@laplace.univ-tlse.fr
4 : |Méso|star>, 4 rue du général Giraud, 31200 Toulouse, France vincent.forest@meso-star.com

Abstract

With this study, we focus on power converters intended for propelling future aircrafts. Currently commercially available power converters do not meet the aeronautical requirements. Even though robust they force designers to oversize the thermal systems. One of the main pain points are the heatsinks or baseplates associated with power modules. Here we propose to get rid of them all together and apply the coolant directly to the semiconductors. This simplifies the design and construction of the modules but, because heat fluxes are really high due to the small footprint of semiconductors, the use of liquid/vapor two phase cooling becomes a necessity. In order to cover this topic, a purposely built module and test loop will be the end target. Before that, more simplified versions of the module will be created to better understand the impact of discrete heat sources on two-phase flow and boiling process. With the same objective, a numerical approach including a Monte Carlo algorithm dealing with complex geometry is proposed.

Introduction

In the scope of electrification - especially in the aeronautical world - reducing the impact of onboarding new power electronic systems is paramount. Every aspect has to be worked on, from EMC to semiconductor but also thermal systems. As really high power (up to 10 MW) starts to be thought to be embedded into aircrafts and even though power converters easily reach 99% efficiency, huge amounts of heat have to be extracted.

Using components on the shelf (COTS) for converters implies deported cooling, i.e. the module and the cooling system are 2 different systems coexisting. This allows for an easy installation but adds thermal resistances between the semiconductors and the cold source.

Previously to this work, Airbus worked on including heatsinks inside the design of the power converter, providing much more efficient cooling but still showing limitations. The first limitation was the brazing of large heatsinks on thin DBC[1] substrates causing warping or even debonding of the copper plates and the MOSFETs[2]. The second is the thermal resistance opposed to the heat flux by the ceramic plates.

With these limitations in mind, we study both experimentally and numerically the use of direct cooling of the semiconductors in a converter like assembly.

Two phase cooling for power electronics has been studied for quite some time using PHPs[3] for space applications [17] or for aircraft applications [18], or capillary driven loops as in [19]. These studies used commercially available electronics but we want to push this approach further by developing a module where the fluid comes in direct contact with the semiconductors.

The reason behind two phase cooling is that it has a minimal geometric impact on the power electronic structure and it will be able to deal with great heat flux density, in our case up to $240\ W.cm^{-2}$.
Due to confinement and surface dry out concerns – detailed below, the fluid will be mechanically pumped through the module.

[1] Direct Bond Copper
[2] Metal-Oxide-Semiconductor Field-Effect Transistor
[3] Pulsating Heat Pipe

1. Experimental Setup

As previously noted, having two-phase flow in direct contact with semiconductors is fairly new to the scientific community. In order to assess the benefits and the drawbacks of this idea, a test bench is currently being built.

1.1. Fluid choice

Because of the particularities of the technology we are exploring, the working fluid used has to be picked carefully. Namely, it has to be Fluor-free, CS-25 compatible, dielectric and present a boiling point as close to 150 °C as possible under atmospheric pressure.

The fluids compatible with these requirements are numerous. In order to assess and rank them, some metrics are needed. The ones used here come from M. Almeida's work [1]. She computes 3 particular merit numbers that are combined into a general one.

First, the pressure drop merit number:

$$C_1 = \frac{\rho_l^{1.75}}{\rho_v} \mu_l^{0.05} \mu_v^{0.2} \qquad (1)$$

Second, the wall overheat in order to initiate boiling:

$$C_2 = \frac{2\sigma}{\rho_l \Delta h} \qquad (2)$$

And finally, the thermal power transported compared to the power consumption of the pump:

$$C_3 = \frac{\rho_v \Delta h}{\rho_l^{0.75} \mu_l^{0.05} \mu_v^{0.2}} \qquad (3)$$

These 3 merit numbers are combined into a general one as follows:

$$C_g = \frac{1}{3}\left[\frac{C_1}{C_{1,max}} + \frac{C_2}{C_{2,max}} + \frac{C_3}{C_{3,max}}\right] \qquad (4)$$

Where $C_{i,max}$ is the maximum of the merit number across all fluids for all temperatures.
As a side note, here each individual merit number is of equal importance compared to the other ones. However if one wishes to prioritize the pump power consumption or low wall overheat to initiate boiling, coefficients can be added to the formula of the general merit number instead of having a straightforward mean value. Also, given the way these numbers are constructed, the lower their value the better the fluid.

We chose to compare 4 different fluids: HFE 7300, HFE 7500, Therminol LT and Dowtherm J. The HFE 7300 and HFE 7500 contain Fluor and will thus not be chosen. They have however been frequently used in previous studies and applications and give a good point of comparison.

Using the data from the manufacturers as well as data from literature, namely [2] for the Ideal Gas Capacity of the HFEs as well as [3] for their viscosities, we were able to plot the following graph. Because Eastman does not provide the surface tension value over the operating temperature range but just at $25\,°C$, a linear approximation was introduced. Meaning $\sigma = 0$ when the temperature reaches the critical point ($377\,°C$ for the Therminol LT).

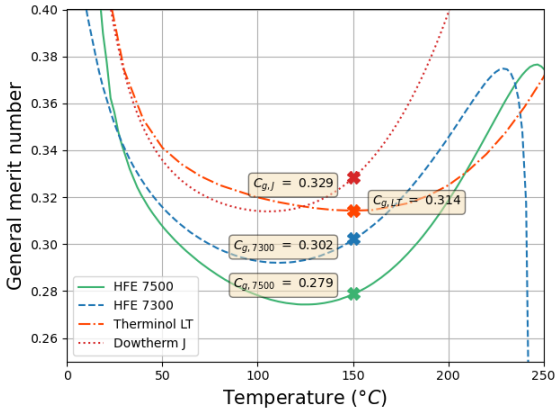

Fig. 1: General merit number of the fluids

At a temperature of $150\,°C$, the fluids perform as follows:

Fluid	General Merit Number	$T_{eb}(P_{atm})$ [°C]
Dowtherm J	0.329	181
Therminol LT	0.314	181
HFE 7300	0.302	98
HFE 7500	0.279	128

Table 1: Fluids General merit numbers

As can be seen in Table 1, the HFE 7500 would be the best fluid to use at $150\,°C$. However – as it contains Fluor – it will not be further considered, which leaves us with the Therminol LT.

1.2. Design of the modules

The heart of this work is the electrical module. As such, it needs to be designed – even in its simplest forms –

as close to an actual power module as possible.
Despite the possibility of using direct two phase cooling on older technologies such as wire bonding, we choose to take full advantage of the emerging technology that are copper bumps [4]. These copper bumps are either copper spheres or cylinders[4] that enable to create the electric stack by interconnecting the upper and lower surfaces. Something that is completely unachievable when using wire bonding. The image below depicts an example of assembly using the bump technology.

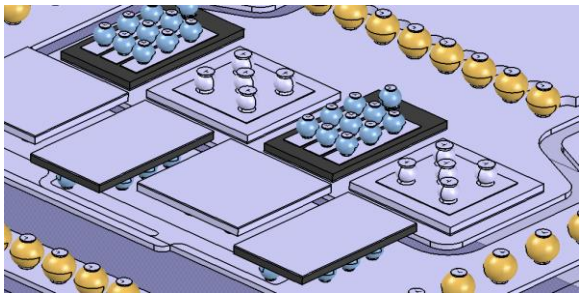

Fig. 2: Example of a power module using spherical bumps

This technology has the advantage of reducing the overall footprint of the module and also – in our case – provides additional exchange surfaces.

However, before testing the module with semiconductors, simpler objects will be assessed. Indeed, in the literature – most of the time – the heating is either realized or considered uniform throughout the object of the study. This can be seen in [5] and [6] using cartridge heaters or in [7] and [8] using ITO[5] films. Because our test loop is brand new, we designed a module using ITO deposit on sapphire glass as can be seen in Fig. 3.

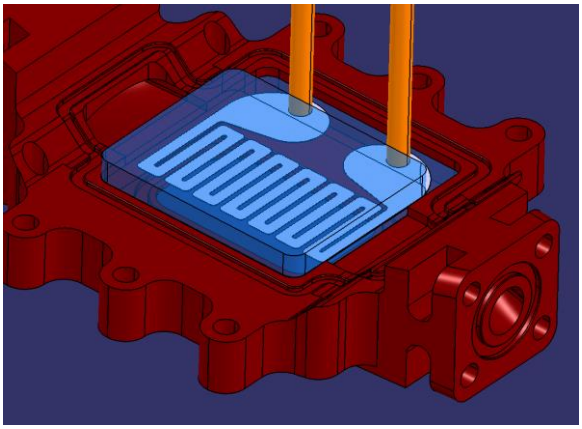

Fig. 3: Opened module using ITO heating

This module is equipped on both sides glass in order for us to take high speed images of the fluid flow, being made out of sapphire they allow for IR measurement.
The final purpose of this internal two-phase flow being

Fig. 4: Working principle of the test loop

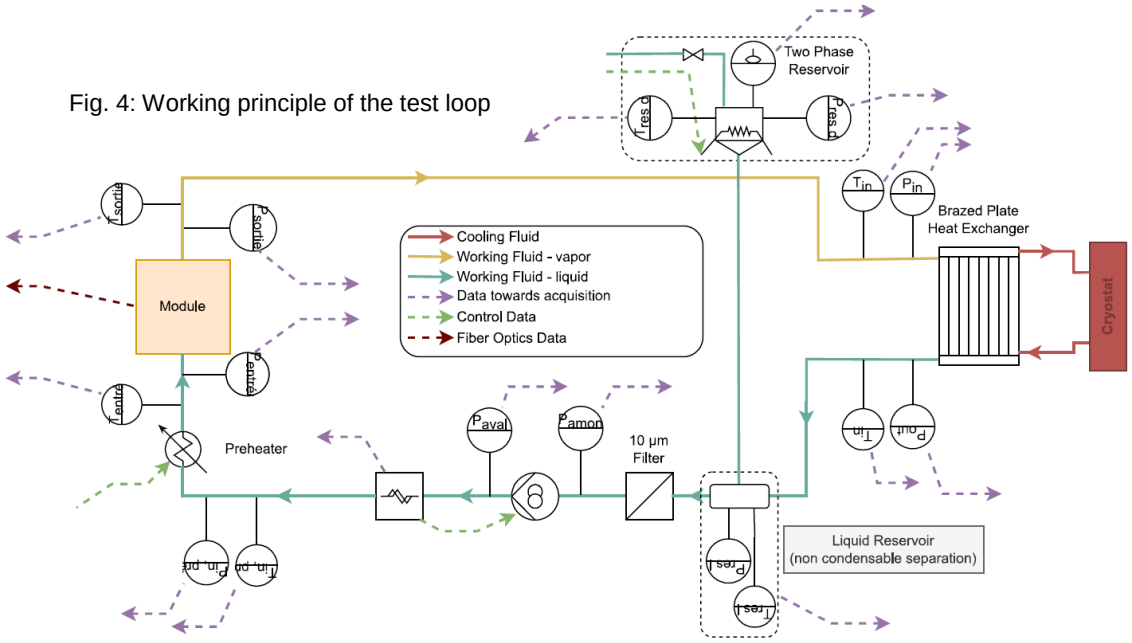

[4] Sometimes called pillars

[5] Indium Tin Oxide

to cool down critical power electronic equipment, reaching CHF[6] – the heat flux density beyond which the wall temperature rises uncontrollably – is not acceptable. In order to avoid CHF and more generally to avoid instabilities, see [5], the module is designed to have a restriction at the inlet as seen in [9] and [10] or rather to have less and less restriction as the liquid turns to vapor inside the module. Here this was implemented not only at module level but rather at loop level. The pipe diameter of the liquid side is $15\ mm$ where the vapor side is $20\ mm$.

The design of the module equipped with semiconductors is not finalized but will integrate the same philosophy. Even though we cannot change the distance between the top and the bottom sapphire glasses, we can shuffle the positions of the bumps so that we have less and less of them the further along the fluid travels inside the module.

1.3. Design of the loop

The working principle of the test bench is analogous to the ones seen in the literature [12], see Fig.4. It is comprised of 2 loops: one with the working fluid, the other with the cooling fluid interfaced with a BPHE[7] used as a condenser.

A mechanical pump will be used, namely a geared pump. A preheater is present close to the entrance of the module in order to closely control the subcooling of the fluid.

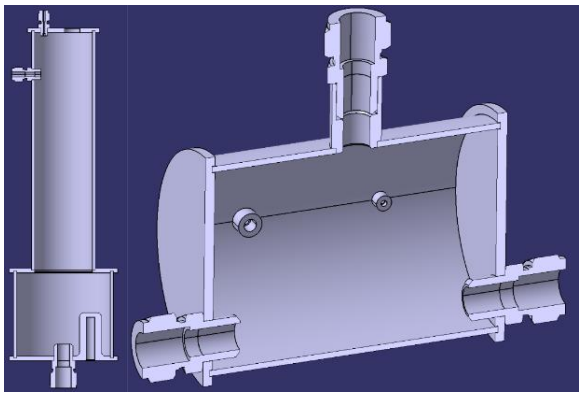

Fig. 5: Cut View of the two-phase reservoir (left) and liquid reservoir (right) – not to scale

Contrary to most systems found in the literature, the two phase reservoir is not in line and a liquid reservoir is added in order to separate the non-condensable gases. As mentioned previously, the semiconductors are rather sensitive, we thus have to closely control the parameters of the fluid. One of the recurrent issues of two phase loop is the presence of non-condensable gases inside the loop.

These gases impact – most of the time negatively – the properties of the fluid. In order to catch and trap them we use what we call a liquid reservoir placed vertically under the two-phase reservoir. The non-condensable gases will thus rise into the latter where we will be able to vent them if and when we want to.

The test bench is currently being setup and will be operational in the coming months. The measurements and insights provided by this loop will allow us to challenge the results from the numerical approach.

2. Numerical approach

In order to optimize the final module, we need to iterate on several positions for the semiconductors and for additional bumps used as thermal and electrical links. The main point of interest in this computation is the junction temperature of the semiconductors. The approach must include the heat transfer with the boiling fluid which is highly dependent of the local heat flux density i.e. of the module geometry. This implies prohibitive costs if each iteration has to be produced and tested.

When dealing with complex geometries, thermal computational advances were recently demonstrated based on a MC[8] algorithm [13]. This is the reason why we explore the coupling of a MC-based code (Stardis [13]) with an averaged model of the two-phase flow inside the module.

2.1 Fluid model

The direct modelling of two-phase flow has been studied for a number of years now but “relies on a number of approximations and empirical parameters that limit the applicability” [14]. Also, in order to grasp the heat exchange, one has to resolve the bubble birth and growth. This is not possible at large module scale with a complex internal geometry.

[6] Critical Heat Flux
[7] Brazed Plate Heat Exchanger
[8] Monte Carlo

For the reasons mentioned above, we choose not to model the full 3D two-phase flow but rather consider it as a well-mixed fluid taken at equilibrium, called the HEM[9]. We develop the equations of this model here after.

2.1.1 *System*

We consider a section of the module dz where $\vec{z}$ is the direction of flow or the normal to any straight section. This system contains two-phase separated by an interface permeable to mass and energy transfers. The model described here considers that values such as the wall temperature and the heat flux density are averaged along the perimeter of the section.

2.1.2 *Hypothesis*

#1 In each and every following equation, the vapor is considered to be at the saturation point. Its temperature is thus a function of the pressure p_v.
#2 The straight section of the module is quasi-uniform and called A.
#3 There is no slip between the phases: $U_v = U_l = U$

This model applies to the modules with the ITO or surface heating. For the modules with semiconductors and bumps, an adaptation of this model will be proposed.

2.1.3 *General Equations*

We have a first equation system describing the homogeneous model in a slice of straight section of our module:

$$\begin{cases} \frac{\partial \rho_m}{\partial t} = -\frac{\partial}{\partial z}[\rho_m U] \\ \frac{\partial}{\partial t}[\rho_m U] = -\frac{\partial}{\partial z}[\rho_m U^2] - \frac{\partial p}{\partial z} + \tau_{w,m}\frac{P_w}{A} + \rho_m \vec{g}.\vec{z} \\ \frac{\partial}{\partial t}[\rho_m H_m] = -\frac{\partial}{\partial z}[\rho_m H_m U] + \langle q_{w,m}\rangle \frac{P_w}{A} + \frac{\partial p}{\partial t} \\ \rho_m = \alpha\rho_v + (1-\alpha)\rho_l \\ \rho_m H_m = \alpha\rho_v H_v^{sat} + (1-\alpha)\rho_l H_l \end{cases} \quad \textbf{(5)}$$

With α, the void fraction:

$$\alpha = \frac{A_v}{A} \quad \textbf{(6)}$$

This form of equation is equivalent to the one we can get when dealing with a compressible monophasic fluid.

2.1.4 *Additional Hypothesis*

So far, in order to write our equations, we have considered the homogeneous behavior, we now also take into account the equilibrium of the two phases:

#4 The two phases are at thermal equilibrium: $T_l = T_v = T(p_{sat})$, thus reducing the number of unknowns.
#5 We admit that the terms associated with the variations of the fluid's properties due to temperature and pressure are negligible compared to the other terms.

2.1.5 *Vapor quality*

We introduce the vapor quality:

$$x = \frac{\dot{m}_v}{\dot{m}_v + \dot{m}_l} = \frac{\rho_v \alpha}{\rho_v \alpha + \rho_l(1-\alpha)} \quad \textbf{(7)}$$

There are two main reasons to introduce x: first is that it allows for a simpler writing of the energy balance equation and second it appears in the parietal friction coefficient and exchange coefficient correlations that will be used.

2.1.6 *Final equations*

Using the vapor quality relation, we have:

$$\begin{cases} \frac{dx}{dz} = \langle q_{w,m}\rangle \frac{P_w}{G\Delta h A} \\ \frac{dp}{dz} = -G^2 \frac{\Delta\rho}{\rho_v \rho_l}\frac{\langle q_{w,m}\rangle}{\Delta h}\frac{P_w}{A} - f_m(x,U)\rho_m U^2 \frac{P_w}{A} + \rho_m \vec{g}.\vec{z} \\ \alpha = \frac{\rho_l x}{\rho_v(1-x)+\rho_l x} \\ \rho_m = \alpha\rho_v + (1-\alpha)\rho_l \\ U = \frac{G}{\rho_m} \end{cases} \quad \textbf{(8)}$$

With $f_m(x,U)$ the wall friction coefficient, U the average flow velocity in a section. G the mass flux is known and in practice is imposed by our pump.

With this final set of equations, we can resolve our system. Once the heat flux density is known – computed from the average wall temperature thanks to Stardis – the first equation can be solved to obtain the vapor quality and the void fraction. Which is then used to solve the pressure equation.

[9] Homogeneous Equilibrium Model

2.2 Solid substrate model

The solid part of our system is modelled by a 3D thermal diffusion equation:

$$\rho_s C_{p,s} \frac{\partial T}{\partial t} - \lambda_s \nabla^2 T = p_{vol} \quad \textbf{(9)}$$

With the following boundary conditions, on any exterior frontier with a $\vec{s}$ normal:

$$\frac{\partial T}{\partial s} = 0 \quad \textbf{(10)}$$

At the solide-fluide interface with a $\vec{s}$ normal:

$$-\lambda_s \frac{\partial T}{\partial s}\Big|_w = h_{eb}(z)[T_{sat} - T_w] \quad \textbf{(11)}$$

The semiconductors have a volumetric power p_{vol}.

2.3 Interfacing the HEM and MC

At their respective core, the HEM and the MC have wildly different ways of computing. The HEM relies on a discretization of the computation domain whereas the MC only relies on a geometric description of the surfaces constituting the volumes of the system.

In order to reconcile these two worlds, we only discretize the wall where the heat exchange between the fluid and the system will occur. For the tests presented here, 100 sections were used to discretize the wall. As a side note, tests were ran on lower number of sections (4, 20 and 50) but lacked precision and induced numerical instabilities that led to the non-convergence of the algorithm.

The computation is coupled in the sense that the data we need from Stardis is the average temperature on each section, this allows the computation of the vapor quality and pressure – in each section – by the HEM which then outputs – through a correlation – the heat exchange coefficient – for each section – that Stardis needs to compute the average temperatures. This whole procedure is referred to as an iteration.
For the results presented here, we used the J.C.Chen correlation [15]:

$$h_{eb} = F(x)h_l + S(x)h_{nb}(x, T_{wall}) \quad \textbf{(12)}$$

The boiling heat transfer coefficient h_{eb} is a function of the vapor quality, the average wall temperature but also of the 2 factors S and F. They respectively represent the suppression of nucleate boiling by forced convective flow and the increase in turbulence due to the two-phase flow.
The average heat flux density used in eq. (8) is linked to this heat transfer coefficient as follows:

$$\langle q_{w,m} \rangle(z) = h_{eb}(z)[T_{sat} - \overline{T_w}] \quad \textbf{(13)}$$

Where $\overline{T_w}$ is the average wall temperature of the considered section.
The iterations are repeated until a satisfactory solution is reached. Once this solution is reached, a final MC computation is launched to obtain the junction temperature of the semiconductors. The general principal of this algorithm is depicted in Fig. 6.

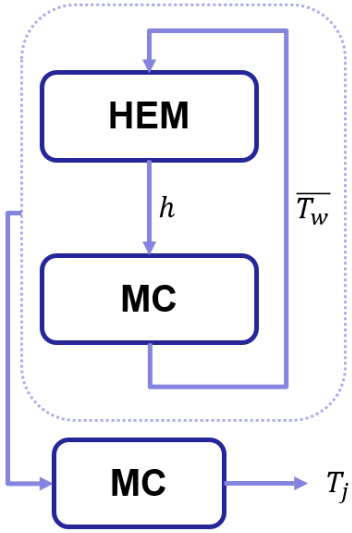

Fig. 6: Numerical scheme of computation

In Fig.7, we can see the highly idealized system that we currently use for our numerical approach. It is comprised of a sapphire tube (transparent) inside of which 6 semiconductors (grey) have been placed.

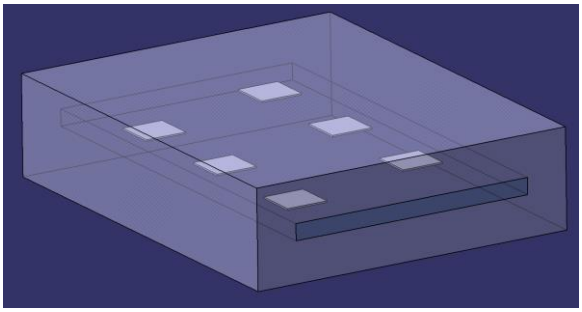

Fig. 7: System used to run simulations

In Fig. 8 and 9, the surface mesh of respectively the sapphire and a section can be seen.

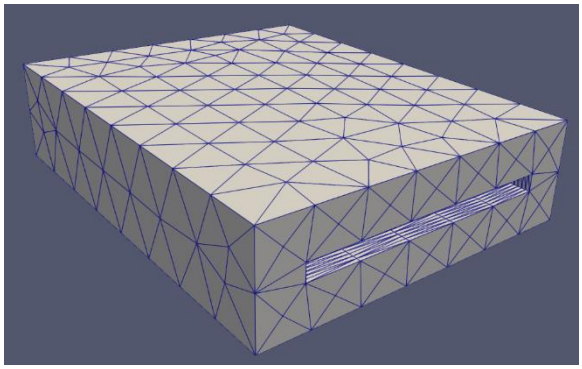

Fig. 8: Surface mesh of the sapphire

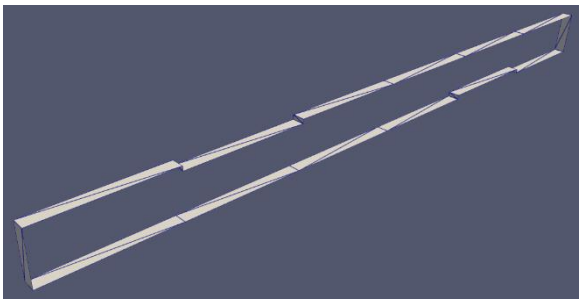

Fig. 9: Surface mesh of one of the section

2.4 Results

Using this correlation the following results were obtained, when using 10 000 MC paths on each section to obtain the mean temperature:

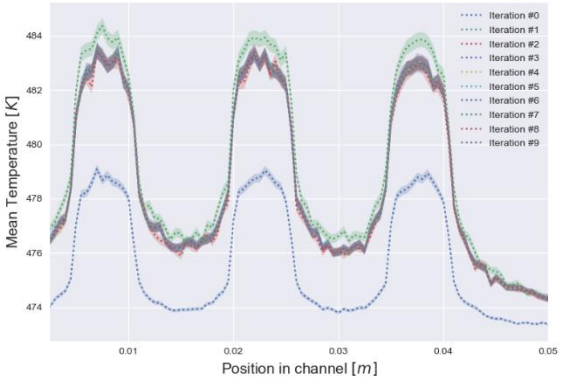

Fig. 10: Mean Temperatures for 10 000 paths

In the graph, Fig. 10, the entry of the module is on the left, $z = 0$. This shows that this approach is able to reach a converged state[10] coherent to what was foreseen in terms of wall temperatures and profile of the curves.

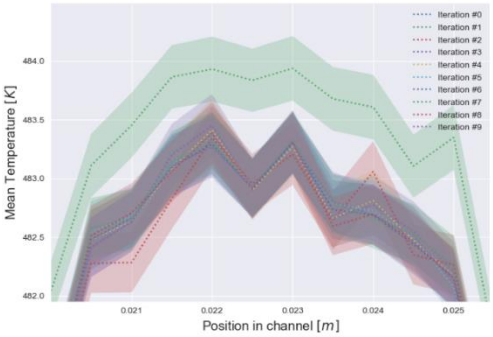

Fig. 11: Zoom of Fig. 10

Even though promising, this result shows sharp temperature variations from one section to the other (see Fig. 11). Because these variations are contained inside the variance[11], we tested the use of 1 million thermal path instead of 10 thousand (see Fig. 12).

The computation with 1 million thermal paths per section showed the same behavior in terms of convergence as the 10 thousand one. This approach was able to fix the sharp variation issue we previously had.

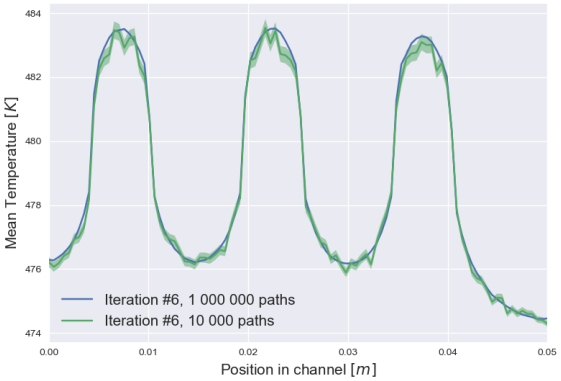

Fig. 12: Comparison between 10 thousand and 1 million thermal paths

It is however not usable practically due to computation time. The 10 thousand paths takes roughly 8 hours of computation on a 8 core laptop whereas the 1 million paths took 7 days on a 32 core station.

[10] Even when drastically changing the initial conditions

[11] A single σ is displayed

2.5 Way forward

The main pain point as of now is the MC algorithm, more especially the time it takes to perform. Because each iteration modifies the heat transfer coefficient we cannot rely on a single MC algorithm but rather we have to redo the whole computation at each iteration. This is an issue because of the computation time of each MC step. Indeed because the sapphire and the semiconductor are highly thermally conductive the probability for the thermal paths to go from conduction to convection is low. This leads to the entrapment of the thermal paths in the solids, explaining the long computation times.

To get rid of this issue, approaches such as the Symbolic Monte-Carlo have been developed, see the work of L.Penazzi [16]. To sum up this methodology, the idea is to launch a first and single MC algorithm on our system but with adapted boundary conditions. This modified algorithm allows us to write the mean temperature as functions of the heat transfer coefficient and the volumetric power of the semiconductors.

Once this – computation heavy – step is done, the iterations can follow as described previously with the major difference that for the MC step, we only compute $T_{wall} = f(h_{eb}, p_{vol})$

This work is still ongoing and will be further explained. Also, because this approach is novel we are currently working on comparing it to a model from AMESIM on a more academic system in order to assess the disparities between our model and a commercial solution.

Conclusions

In this paper we described our decision making process regarding the fluid and our approach to designing the modules, coming from a “classic” uniform heating, uniform straight section towards a discretely heated with non-uniform straight section. Taking advantage of the copper bump technology as well as the advances in flow stability.

We covered the numerical approach that was used to obtain promising results but lack scalability. The Symbolic Monte-Carlo method was introduced and will be implemented to alleviate this issue. The CHF also needs to be acknowledge and will be implemented into the algorithms.

References

1 M. Almeida. Etude des écoulements diphasiques pour le refroidissement des composants électroniques en systèmes embarqués. Mécanique des fluides. Université Grenoble Alpes (2019)

2 A. Aminian et al. Ideal Gas Heat Capacity and Critical Properties of HFE-Type Engineering Fluids: Ab Initio Predictions of Cpig, Modeling of Phase Behavior and Thermodynamic Properties Using Peng–Robinson and Volume-Translated Peng–Robinson Equations of State. Int J Thermophys 43, 87 (2022).

3 Michael H. Rausch et al. Density, Surface Tension, and Kinematic Viscosity of Hydrofluoroethers HFE-7000, HFE-7100, HFE-7200, HFE-7300, and HFE-7500 Journal of Chemical & Engineering Data 60 (12), 3759-3765 (2015)

4 A. Castellazzi. Power Device Stacking using Surface Bump Connections. 2009 21st International Symposium on Power Semiconductor Devices & IC's 204-207 (2009)

5 K. Satish et al. Experimental Study of Flow Patterns, Pressure Drop, and Flow Instabilities in Parallel Rectangular Minichannels. Heat Transfer Engineering - HEAT TRANSFER ENG. 26. 20-27 (2005)

6 W. Qu et al. Flow boiling heat transfer in two-phase micro-channel heat sinks — I. Experimental investigation and assessment of correlation methods, International Journal of Heat and Mass Transfer, Volume 46, Issue 15 (2003)

7 H. Seo et al. Pool boiling CHF of reduced graphene oxide, graphene, and SiC-coated surfaces under highly wettable FC-72, International Journal of Heat and Mass Transfer, Volume 82 (2015)

8 C. Baldassari et al. Non-Uniform Onset of Nucleate Flow Boiling of R-134a Inside a Glass Minichannel, Experimental Heat Transfer, 27:4 (2014)

9 G. Hedau et al, Combined effect of inlet restrictor and nanostructure on two-phase flow performance of parallel microchannel heat sinks, International Journal of Thermal Sciences, Volume 153, (2020)

10 S. K. Oudah et al. An experimental investigation of the effect of multiple inlet restrictors on the heat transfer and pressure drop in a flow boiling microchannel heat sink. International Journal of Heat and Mass Transfer, 153 :119582, (2020)

11 P. Zhang et al, Review of recent developments on pump-assisted two-phase flow cooling technology, Applied Thermal Engineering (2019)

12 J.M. Tregan et al, Coupling radiative, conductive and convective heat-transfers in a single Monte Carlo algorithm: A general theoretical framework for linear

situations PLOS ONE 18(4): e0283681 (2023)
13 http://meso-star.com/projects/stardis/stardis.html
14 G. Giustini. Modelling of Boiling Flows for Nuclear Thermal Hydraulics Applications — A Brief Review. *Inventions*, *5*, 47 (2020)
15 J. C. Chen. Correlation for Boiling Heat Transfer to Saturated Fluids in Convective Flow. Industrial & Engineering Chemistry Process Design and Development 5 (3), 322-329 (1966)
16 L. Penazzi et al. Toward the use of Symbolic Monte Carlo for Conduction-Radiation Coupling in Complex Geometries. RAD-19 - 9th International Symposium on Radiative Transfer, Jun 2019, Athens, Greece. 8 p., ff10.1615/RAD19.380
17 L. Pietrasanta, A pulsating heat pipe embedded radiator: Thermal-vacuum characterisation in the pre-cryogenic temperature range for space applications, Thermal Science and Engineering Progress, Volume 19 (2020)
18 F. Accorinti, Two-Phase Power Electronics Cooling Solution Design in Air Context Answering to the Objectives of the Hybrid Aircraft 2035, Theses (2020)
19 E. Videcoq et al, On-line thermal regulation of a capillary pumped loop via state feedback control using a low order model, Applied Thermal Engineering, Volume 108 (2016)

Nomenclature

A	Straight section $[m^2]$
C_p	Heat Capacity $[J.K^{-1}kg^{-1}]$
F	Forced convection factor $[1]$
G	Mass flux $[kg.s^{-1}.m^{-2}]$
g	Gravity $[m.s^{-2}]$
H	Enthalpy $[kJ.kg^{-1}]$
P_w	Wall perimeter in a section $[m]$
p	Pressure $[Pa]$
q	Heat Flux density $[W.m^{-2}]$
S	Suppression factor $[1]$
T	Temperature $[K]$
U	Velocity $[m.s^{-1}]$
x	Vapor quality $[1]$
z	Space coordinate $[m]$
Δh	Enthalpy of vaporization $[kJ.kg^{-1}]$
α	Void fraction $[1]$
μ	Dynamic Viscosity $[kg.m^{-1}.s^{-1}]$
ρ	Density $[kg.m^{-3}]$
σ	Surface Tension $[N.m^{-1}]$
τ	Parietal friction $[kg.m^{-1}.s^{-2}]$

Sub- Superscript

m	Mean value taken on a section
l	Refers to liquid phase
v	Refers to vapor phase
s	Refers to the solid
sat	Value taken at saturation point
eb	Refers to ebullition
nb	Refers to nucleate boiling
w	Value taken at wall contact